Effect of Ta on the structural, thermodynamic and elastic properties of FCC Pt-W-Ta alloys – first-principles study

Kedibone Lekganyane[1*], *Malika* Khodja-Moller[1], *Roelof* Mostert[1], *Donald* Mkhonto[2], and *Maje* Phasha[2]

[1]Department of Materials Science and Metallurgical Engineering, University of Pretoria, Private Bag X20, Hatfield, 0028, South Africa.
[2]Advanced Materials Division, MINTEK, Private bag X 3015, Randburg, 2125, South Africa

Abstract. This study employs density functional theory (DFT) to predict the mechanical properties of ternary Pt-W-Ta alloys with concentrations of up to 10 at.%. The binary FCC Pt-10W alloy served as a benchmark to assess the effects of Ta additions. All studied alloys were FCC structures and were thermodynamically and mechanically stable. Pt-7W-3Ta alloy exhibited higher elastic moduli than Pt-10W and Pt-3W-7Ta, making it suitable for durable jewellery components. Hardness increased with increasing Ta content at the expense of ductility. Pt-3W-7Ta displayed higher hardness than Pt-10W and Pt-7W-3Ta.

1 Introduction

The resistance of jewellery to wear, scratches, denting, and deformation is primarily determined by the hardness of the alloy [1]. Corti's survey highlighted that soft to moderately hard platinum alloys, with hardness values between 50 and 150 HV, are more susceptible to shape deformation, scratches, and dents [1]. Alloys with hardness values between 150 and 170 HV offer sufficient wear and scratch resistance [2]. However, for alloys requiring adequate spring properties, hardness values between 300 and 450 HV are essential. Spring properties enhance the holding power of gemstones and increase the number of cycles the piece can withstand during use, making them vital for applications such as bracelet closure clips, omega clips, ear nut clasps, prong settings, and earring posts. To achieve this, the current study selected refractory elements, namely, tungsten (W) and tantalum (Ta), as potential hardening alloying elements.

When added to platinum (Pt), tungsten enhances hardness through solid solution and precipitation strengthening, while tantalum refines the microstructure and improves mechanical properties. The high melting points of W and Ta render the alloy unsuitable for conventional casting methods, making additive manufacturing (AM), specifically Selective Laser Melting (SLM), a promising alternative [3].

* Corresponding author: Kedibonel@mintek.co.za

AM enables precise microstructural control and potentially superior mechanical performance in these high-temperature alloys [3]. In this study, density functional theory (DFT)-based first principles quantum mechanics calculations were employed to generate structural, thermodynamic, and elasticity data for face-centred cubic (FCC) ternary Pt-W-Ta alloy compositions, with tungsten and tantalum concentrations explored up to approximately 10 atomic per cent (at.%). Using the binary FCC Pt-10W alloy [4] as a benchmark, this approach allows us to assess the impact of Ta additions on the mechanical properties of Pt-W-Ta alloys with combined W and Ta concentrations of up to 10 at.%. Due to the high mutual solubility of tungsten and tantalum, they can either dissolve within the Pt matrix or form second-phase particles during age hardening, enhancing stiffness, strength, and hardness to improve the alloy's suitability for jewellery applications.

The results obtained from the DFT-based CASTEP code predict the intrinsic properties of a perfectly ordered structure immediately after solidification, assuming ideal thermodynamic equilibrium. These properties include the lattice parameter, formation enthalpy, and elastic moduli. It is important to note that this study is computational and does not include experimental validation of the predicted properties. The findings represent the ideal ground-state behaviour (0 K) of Pt-W-Ta solid solutions, and the trends observed in thermodynamic stability, elastic moduli, and lattice distortion provide valuable theoretical insights into the intrinsic behaviour of these alloys.

2 Computational methods

In this study, the structural, thermodynamic, and elastic properties of ternary FCC Pt-W-Ta solid solution alloys were examined using first-principles calculations based on DFT. These calculations were performed with the CASTEP module integrated into the Materials Studio software suite [5, 6]. The associated crystal structures are illustrated in Figure 1. To model ion-electron interactions, Vanderbilt ultrasoft pseudopotentials [7] were deployed, combined with the generalised gradient approximation (GGA) [8] in the Perdew-Burke-Ernzerhof (PBE) functionality [9] and Pt_00PBE.usp pseudopotentials.

2.1 Crystal configurations and simulation parameters.

The research analysed three face-centred cubic (FCC) crystal models: a unit cell, 2×2×2 and 3×3×3 supercells, all classified under space group #221 (Pm3m). These models consisted of 4 atoms for the unit cell, 32 atoms for pure Pt and binary Pt-W, and 108 atoms for the Pt-W-Ta ternary configurations. A consistent plane-wave cut-off energy of 750 eV was applied across all configurations. For Brillouin zone sampling, a 24×24×24 k-point mesh was employed for the unit cell, while a finer 7×7×7 mesh was used for the benchmark binary $Pt_{32-x}W_x$ supercell [4]. For the ternary $Pt_{108-x-y}W_xTa_y$ supercells, a 4×4×4 grid was selected to ensure sufficient total energy convergence.

The equilibrium structures were determined through geometry optimisation using the Broyden–Fletcher–Goldfarb–Shanno (BFGS) algorithm [10]. Optimisation was guided by strict convergence conditions: energy changes below 1 x 10^{-5} eV per atom, residual forces not exceeding 0.03 eV/Å, bulk stress limited to 0.05 GPa, and maximum atomic displacements confined to 1 x 10^{-3} Å. For each alloy system, structural relaxation was performed to obtain the most stable configuration. These optimised geometries were subsequently used to evaluate the elastic constants, which were then applied to predict the mechanical performance of the binary Pt-W [4] and ternary Pt-W-Ta FCC solid solution alloys.

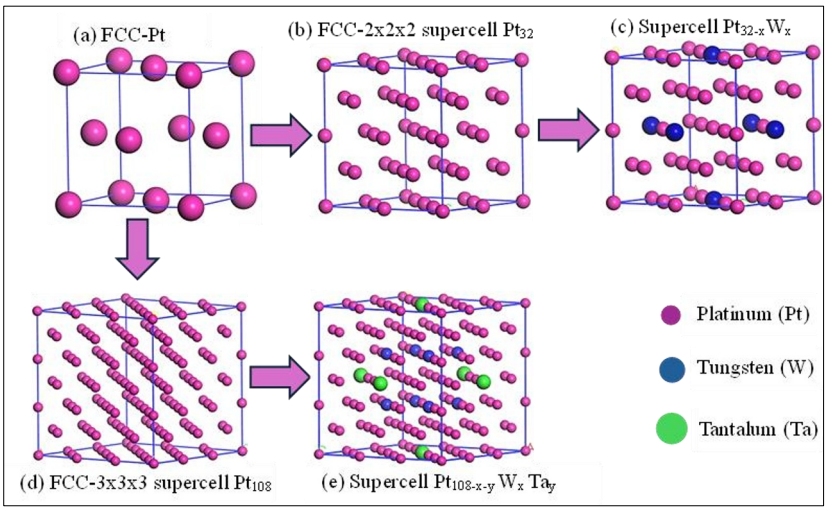

Fig. 1. Schematic representation of (a) FCC Pt unit cell and (b) 2×2×2 supercell crystal structures of (c) Pt_{32}-xW_X [4] and (d) 3x3x3 supercell crystal structure of (e) $Pt_{108-x-y}$ W_xTa_y

3 Thermodynamic properties

Formation enthalpy is a fundamental metric used to assess the likelihood of crystal structure formation and the thermodynamic stability of alloy systems [11–13]. In this study, the calculation of ΔH_f considers the composition-dependent contributions of W and both W and Ta.

For example, Equation (1) defines the formation enthalpy of the binary Pt-W [4] alloy as the difference between the total energy of the alloy and the sum of the DFT total energies per atom of pure Pt and W, scaled by their respective atomic fractions. A negative ΔH_f value indicates that alloy formation is energetically favourable compared to the separate elemental states.

$$\Delta H_f^{Pt_{n-x}W_x} = \frac{E_{Total}^{Pt_{n-x}W_x}}{n} - \left[\frac{(n-x)}{n}.E_{pure}^{Pt} + \frac{x}{n}.E_{pure}^{W}\right] \quad (1)$$

$$\Delta H_f^{Pt_{n-x-y}W_xTa_x} = \frac{E_{Total}^{Pt_{n-x-y}W_xTa_x}}{n} - \left[\frac{(n-x-y)}{n}.E_{pure}^{Pt} + \frac{x}{n}.E_{pure}^{W} + \frac{y}{n}.E_{pure}^{Ta}\right] \quad (2)$$

The values *x* and *y* indicate the number of W and Ta atoms, while the expressions *(n−x)/n* and *(n-x-y)/n* define the atomic fractions of platinum in the binary and ternary systems, respectively. E^{Pt}, E^{W}, and E^{Ta} represent the total energies of elemental Pt, W, and Ta in their respective ground-state crystal structures.

Equation (2) extends the formation enthalpy calculation to the ternary Pt-W-Ta system. It accounts for the energy contributions from all three elements—Pt, W, and Ta—each weighted by their atomic proportions. This allows for evaluating how the simultaneous presence of W and Ta influences the alloy's thermodynamic stability.

4 Elastic properties

Elastic constants are fundamental to describing a material's mechanical behaviour and are used to calculate moduli such as the shear modulus (G), Poisson's ratio (ν), bulk modulus (B), and Young's modulus (E). These moduli offer valuable insights into intrinsic mechanical properties such as stability, anisotropy, ductility, hardness, brittleness, and stiffness [14]. In this study, the elastic constants were determined by applying a linear fit to the stress–strain response based on Hooke's law [15,16]. Since the Pt-W and Pt-W-Ta alloys crystallise in a cubic structure, they are characterised by three independent second-order elastic constants: C_{11}, C_{12}, and C_{44}.

4.1 The elastic stability criteria

The Born stability criteria [17] are a set of conditions derived from the elastic constants of a crystal that determine its mechanical stability under small deformations. For cubic crystals, such as the FCC Pt-W and Pt-W-Ta alloys investigated in this study, the criteria require that the following inequalities be satisfied: $C_{11} > 0$, C_{11}-$C_{12} > 0$, C_{11}+2$C_{12} > 0$, and $C_{44} > 0$. These conditions ensure that the crystal can resist shear and volumetric deformations without undergoing spontaneous structural changes. Specifically, C_{11}-$C_{12} > 0$ addresses the shear stability along {100} planes, C_{11}+2$C_{12} > 0$ relates to the bulk modulus and overall volume stability, and $C_{44} > 0$ guarantees resistance to shear along other crystallographic directions.

Elastic behaviour describes the ability of a crystalline solid to deform reversibly under small external forces. This property is vital for applications such as jewellery, where materials are expected to retain shape while offering resilience and flexibility. In this study, elastic properties were computed using first-principles calculations by applying small strains to the optimised structures and deriving the stress–strain relationship. From the second-order elastic constants, isotropic elastic moduli were estimated using the Voigt-Reuss-Hill (VRH) approximation [18], which averages the theoretical Voigt's upper [19] and Reuss's lower bounds [20] of bulk and shear moduli to provide realistic estimates for polycrystalline behaviour according to the following equations:

$$B_{VRH} = \frac{(B_V + B_R)}{2} \tag{3}$$

Where B_{VRH} is Hill's average arithmetic mean for bulk modulus, and $B_V = B_R$, where B_V is the Voigt upper bound for bulk modulus and B_R is the Reuss lower bound for bulk modulus.

$$B_V = \frac{C_{11} + 2C_{12}}{3} \tag{4}$$

and

$$G_{VRH} = \frac{G_V + G_R}{2} \tag{5}$$

Where G_{VRH} is the Hill's average arithmetic mean for shear modulus. G_V is the Voigt upper bound for shear modulus, and G_R is the Reuss lower bound for shear modulus and are given by the following equations:

$$G_V = \frac{C_{11} - C_{12} + 3C_{44}}{5} \tag{6}$$

$$G_R = \frac{5C_{44}(C_{11} - C_{12})}{4C_{44} + 3(C_{11} - C_{12})} \tag{7}$$

From the Hill-averaged bulk modulus, B_{VHR} and shear modulus G_{VHR}, Young's modulus, E and Poisson's ratio, υ were calculated using the following relations:

$$E = \frac{9B_{VRH} \times G_{VRH}}{3B_{VRH} + G_{VRH}} \quad (8)$$

$$v = \frac{3B_{VRH} - 2G_{VRH}}{2(3B_{VRH} + G_{VRH})} \quad (9)$$

Poisson's ratio offers valuable information about how a material deforms under stress before breaking. Generally, materials exhibiting a higher Poisson's ratio are more capable of plastic deformation, indicating ductile behaviour. In contrast, lower values are often linked to brittleness. A Poisson's ratio below 0.26 typically signifies brittle characteristics, whereas higher values suggest increased ductility.

These mechanical parameters provide key insights into the alloy's stiffness, rigidity, compressibility, ductility, hardness and machinability. All results were obtained in the 0 K ground-state configuration, consistent with the predictive nature of DFT simulation. Additionally, ductility of binary FCC Pt-W and ternary Pt-W-Ta alloys was calculated using Pugh's ratio [21]. This ratio is denoted by k and is defined as the ratio of the bulk modulus (B_{VRH}) and shear modulus (G_{VRH}) according to the following equation:

$$k = \frac{B_{VRH}}{G_{VRH}} \quad (10)$$

A Pugh's ratio greater than 1.75 typically indicates ductile behaviour, while lower values suggest brittleness. The Vickers hardness was further estimated using the empirical model proposed by Liu et al. [22], which relates hardness to the shear modulus:

$$Hv = 0.92 \times k^{1.137} \times G^{0.708} \quad (11)$$

where HV is the predicted hardness (GPa), G_{VRH} is the shear modulus, and $k = G_{VRH}/B_{VRH}$. To estimate the solid-state workability of the alloys under ideal conditions, the machinability index was calculated using elastic constants obtained from 0 K first-principles simulations. Following the approach by Hoover and Sun et. al. [23, 24], the machinability index reflects shear resistance on specific slip systems. The machinability index is denoted by μ and is defined as the ratio of the bulk modulus, B, to the elastic stiffness constant, C_{44} according to:

$$\mu = \frac{B_{VRH}}{C_{44}} \quad (12)$$

A higher machinability index typically correlates with better material workability, which is a desirable trait for jewellery manufacturing processes involving cutting, forming, or polishing. All property predictions were performed at 0 K using fully relaxed, ground-state structures. Zener's anisotropy index, A_Z, [25] is a useful parameter for quantifying the elastic anisotropy of a cubic crystal, and it is defined by the following equation:

$$A_Z = \frac{2C_{44}}{C_{11} - C_{12}} \quad (13)$$

For a perfectly isotropic material**,** the value of A_Z is exactly one. Values deviating from one indicate elastic anisotropy, with larger deviations suggesting greater differences in mechanical response along different crystallographic directions. This index is particularly important in evaluating how a material may behave under complex stress states. In the context of jewellery alloys, anisotropy plays a role in how the material responds to forming processes and mechanical wear, especially in small and intricate components. The Universal Anisotropy Index, A_U [26] provides a comprehensive measure of elastic anisotropy by accounting for both shear and bulk modulus contributions. A_U is expressed as:

$$A_U = \frac{5G_V}{G_R} + \frac{B_V}{B_R} - 6 \tag{14}$$

where G_V and G_R are the Voigt and Reuss shear moduli, and B_V and B_R are the Voigt and Reuss bulk moduli. A material is considered elastically isotropic if $A_U = 0$. Any deviation from zero reflects the presence of elastic anisotropy, with larger values indicating greater differences in mechanical response across crystallographic orientations. Unlike Zener's index, which is limited to cubic systems, A_U is applicable to all crystal symmetries, making it a more general tool for assessing directional mechanical behavior. This is especially valuable for jewellery applications where consistent performance under multi-axial stress is essential.

5 Results and discussions

5.1 Structural properties

The results reveal a clear trend of increasing lattice parameters with increasing Ta content, relative to the Pt-10W baseline, see Table 1 column 2. This expansion is attributed to the larger atomic radius of Ta (0.146 nm) compared to both W (0.141 nm) and Pt (0.139 nm), resulting in enhanced lattice distortion when Ta substitutes into the Pt lattice. Importantly, all compositions maintain a face-centred cubic (FCC) structure with no indication of phase transformation under ground-state conditions, confirming the crystal structure stability. The smooth increase in lattice parameter and absence of structural disruption suggest good solubility of Ta and W in Pt. This is further supported by the known complete mutual solubility of W and Ta, both of which crystallise in the BCC structure and share similar atomic sizes and electronic properties. These characteristics promote stable substitutional behaviour within the Pt matrix.

The substitution of larger atoms (particularly Ta) introduces greater lattice strain and distortion compared to W alone, which enhances solid solution strengthening. As such, the Ta-containing alloys, especially Pt-3W-7Ta, are expected to exhibit greater hardness and strength than the benchmark Pt-10W, due to increased resistance to dislocation motion.

5.2 Formation enthalpy

In Table 1, column 3, the heats of formation show a clear trend of increasing thermodynamic stability with increasing Ta content, relative to the Pt-10W benchmark. While Pt-10W is stable due to the known solubility of W in Pt, the introduction of Ta significantly lowers the formation enthalpy, indicating stronger bonding and enhanced stability of the solid solution. This aligns with the fact that both W and Ta are mutually soluble in Pt and with each other.

The more negative ΔH_f values suggest that Ta addition not only improves lattice distortion for mechanical strengthening but also enhances the alloy's chemical stability, making Pt-W-Ta alloys promising for demanding applications like wear-resistant jewellery.

Table 1. The calculated lattice parameter, a (Å) and heats of formation for binary FCC Pt-W, Pt-7W-3Ta and Pt-3W-7Ta alloys

Platinum alloy composition (at. %)	**Lattice Parameter, a (Å)**	**Heats of Formation ΔH_f (KJ/mol)**
Pt-10W [4]	3.993	-11.3 [4]
Pt-7W-3Ta	3.998	-20.4
Pt-3W-7Ta	4.009	-25.8

5.3 Elastic constants

Table 2 presents the computed elastic constants for various platinum alloy compositions, which are essential for evaluating their mechanical properties in jewellery applications. The Pt-W, Pt-7W-3Ta and Pt-3W-7Ta alloys adopt an FCC crystal structure.
These elastic constants ensure that the material resists elastic deformation under various stress states and do not exhibit any internal lattice instabilities under small perturbations. All the Pt-W-Ta alloys investigated in this study possess positive values and fulfil Max Born's criteria, confirming that the FCC crystal structure remains mechanically stable under ground-state conditions.

In comparison to the Pt-10W benchmark, both Pt-7W-3Ta and Pt-3W-7Ta alloys exhibit enhanced mechanical properties, including increased stiffness and shear resistance, contributing to their overall elastic performance. However, Pt-7W-3Ta stands out as the most advantageous composition for applications demanding high mechanical stability and performance, while Pt-3W-7Ta still offers improvements over Pt-10W but to a slightly lesser extent. The observed variation in the C_{12} elastic constant among the Pt-based alloys highlights the subtle influence of tantalum addition on the alloy's transverse mechanical response. Notably, Pt-3W-7Ta exhibits a slightly lower C_{12} value (222 GPa) compared to Pt-10W (223 GPa), indicating a minor reduction in resistance to lateral deformation under uniaxial stress.

This suggests that higher Ta content may reduce the effectiveness of interatomic bonding in constraining transverse strain, possibly due to differences in atomic bonding character between Ta and W in the FCC Pt matrix. Conversely, Pt-7W-3Ta displays the highest C_{12} value (234 GPa), reflecting a well-balanced alloy composition that enhances both longitudinal and transverse stiffness. This balance is particularly advantageous for jewellery applications where mechanical integrity under cyclic loading and dimensional stability are critical. These insights can guide material selection for specific jewellery applications based on desired mechanical properties.

Table 2: The computed second-order elastic constants of Binary FCC Pt-W alloy and Ternary FCC Pt-W-Ta alloys.

Composition	C_{11} (GPa)	C_{12} (GPa)	C_{44} (GPa)	$C' = (C_{11}-C_{12})/2$ (GPa)
Pt-10W [4]	331	223	97	54
Pt-7W-3Ta	348	233	111	57
Pt-3W-7Ta	336	222	109	57

5.4 Elastic moduli

The elastic moduli serve as critical indicators of mechanical performance in platinum jewellery alloys, governing essential characteristics including deformation resistance, ductility, fatigue life, and spring properties. These parameters directly determine a jewellery piece's functionality and longevity, particularly in demanding applications such as stone settings, earring nuts, clasps, and clips, where optimal springback and cyclic loading resistance are paramount. These elastic Moduli include but are not limited to the bulk modulus (B), shear modulus (G), Young's modulus (E), and Poisson's ratio (ν).

For instance, while B and G dictate the alloy's intrinsic response to compressive and shear stresses in prong settings, E and ν influence both the stiffness required for securing stone retention and the spring characteristics needed for reliable clasp operation. Our density functional theory calculations reveal how tantalum strategically modifies these elastic properties in Pt-W alloys. Equations (3)-(9) were used to calculate the elastic moduli.

Table 3 shows the elastic moduli and mechanical properties of pure platinum, Pt-W and Pt-W-Ta alloys. From the results obtained, the addition of Ta to Pt-W alloys induces substantial improvements in mechanical properties over pure platinum and binary Pt-10W. While pure Pt exhibits excessive ductility ($B/G = 4.8$, $\nu = 0.40$) and inadequate hardness (2.60 GPa), the Pt-10W alloy enhances stiffness ($E = 209$ GPa) and hardness (4.97 GPa) but is constrained by tungsten's solubility limits and diminishing strengthening effects.

The introduction of 3 at. % Ta (Pt-7W-3Ta) optimizes this system, achieving superior hardness (5.75 GPa), elastic modulus (232 GPa), and shear resistance ($G = 85$ GPa) while retaining ductility ($B/G = 3.2$, $\nu = 0.36$) and these properties are ideal for high-stress jewellery components such as prongs, bands, and settings. However, excessive Ta addition of 7 at.% (Pt-3W-7Ta) leads to diminishing returns: hardness plateaus (5.88 GPa), bulk modulus declines (260 GPa vs. 272 GPa in Pt-7W-3Ta), and ductility reduces ($B/G = 3.1$, $\nu = 0.35$). This was expected, as the elastic constants of these alloys, although possessing positive values, were low as compared to the elastic constants for Pt-7W-3Ta alloy.

Critically, Pt-7W-3Ta demonstrates exceptional fatigue resistance and spring properties, making it suitable for cyclic-load applications (e.g., clasps, earring nuts) whereas Pt-3W-7Ta risks crack propagation due to its reduced stiffness and ductility or fracture toughness. This is corroborated by Pugh's ratio (B/G) and Poisson's ratio (ν), which confirm Pt-7W-3Ta's balanced deformability, whereas Pt-3W-7Ta may be on the borderline of ductile-to-brittle transition because of the intrinsic factors such as lattice distortion, phase separation, mixed bonding strength, and competing strengthening mechanisms.

Table 3: Elastic moduli and mechanical properties of pure Pt, Pt-W, and Pt-W-Ta.

Property	Pure Pt [4]	Pt-10W[4]	Pt-7W-3Ta	Pt-3W-7Ta
Bulk Modulus (B, GPa)	256	259	272	260
Shear Modulus (G, GPa)	53	77	85	84
Young's Modulus (E, GPa)	150	209	232	228
Poisson's ratio (υ)	0.40	0.37	0.36	0.35
Pugh ratio (B/G)	4.8	3.4	3.2	3.1
Hardness (HV)	2.60	4.97	5.75	5.88

The machinability, Zener anisotropy, and universal anisotropy indices provide additional insight into the processability and mechanical performance of the Pt-W and Pt-W-Ta alloys. As shown in Table 4, Pt-10W exhibits the highest machinability (2.67), making it the easiest to fabricate, while increasing Ta content slightly reduces machinability due to enhanced lattice distortion and solid solution strengthening. Nevertheless, all alloys maintain hardness values within the optimal 3–8 GPa range, which ensures adequate damage tolerance and workability for jewellery manufacturing.

Among the Pt-W-Ta alloys studied, both the Zener and universal anisotropy indices show that elastic anisotropy increases relative to the Pt-10W benchmark. Notably, the slightly higher universal anisotropy index ($A_U = 0.547$) for the Pt-7W-3Ta alloy, compared to Pt-3W-7Ta ($A_U = 0.528$), suggests a marginally increased directional dependence in its elastic behaviour. This rise in anisotropy may be influenced by the specific atomic-scale interactions between W and Ta at lower Ta concentrations**,** which may lead to less uniform distribution of local stiffness across crystallographic directions. Despite this, Pt-7W-3Ta still exhibits a favourable combination of mechanical properties, such as higher elastic constants and machinability, making it a more viable alloy for jewellery applications where reliability and spring-like behaviour are essential**.**

Table 4 : Machinability, Zener anisotropy and universal anisotropy indices of Pt-W [4] and Pt-W-Ta alloys.

Alloy composition	Machinability index, μ	Zener anisotropy, A_Z	Universal anisotropy index, A_U
Pt-10W [4]	2.67	1.80	0.427
Pt-7W-3Ta	2.44	1.94	0.547
Pt-3W-7Ta	2.38	1.92	0.528

6 Conclusion

The Pt-10W and Pt-W-Ta alloys examined in this study all crystallise into a stable face-centred cubic (FCC) crystal structure under ground-state conditions, with no indication of phase transformations. The increasingly negative heats of formation with higher Ta content suggest enhanced thermodynamic stability, attributed to solid solution strengthening and the high mutual solubility of W and Ta in the Pt matrix. The computed elastic constant analysis reveals that moderate Ta addition, as in Pt-7W-3Ta, significantly improves stiffness and shear resistance, which is evident in the elevated values of C_{11}, C_{12}, C_{44}, and C' without destabilising the crystal structure. Relative to the Pt-10W baseline, the addition of Ta not only promotes lattice expansion but also results in marked improvements in mechanical performance while preserving phase stability.

Further mechanical evaluation through elastic moduli comparisons confirms the positive impact of Ta incorporation. As 3 at. % of Ta replaces the W atoms in Pt-10W alloy, B, G, and E increase, indicating greater resistance to elastic deformation. In contrast, Pt-3W-7Ta, while offering the greatest hardness and still superior stiffness relative to Pt-10W, exhibits signs of reduced ductility, as seen in the lower Poisson's ratio and B/G ratio, which are key indicators of a potential shift toward brittleness. This trade-off raises concerns for applications like jewellery, where both durability and workability are essential.

The machinability index suggests that although Pt-10W is the easiest to process, the slight reduction in machinability observed in Ta-containing alloys (i.e the ternaries) remains within acceptable limits (3–8 GPa hardness range) for jewellery applications. Both the Zener anisotropy (A_Z) and the Universal Anisotropy Index (A_U) increase slightly with Ta addition, with Pt-7W-3Ta showing a marginally higher A_U than Pt-3W-7Ta, indicating a modest directional dependence of mechanical response. Despite this observation, the Pt-7W-3Ta alloy strikes a favourable balance of combining high elastic performance, good processability, and tolerable anisotropy, making it the most promising candidate for demanding jewellery components such as closure and opening clips, omega clips, earnout clasps, prongs settings, and earring posts that require fatigue resistance and spring-like properties.

The author gratefully acknowledges the financial support provided by Mintek and the Advanced Metals Initiative (AMI) of the Department of Science and Innovation (DSI), South Africa. Special thanks are extended to all supervisors at the University of Pretoria and Mintek for their valuable guidance and support. Sincere appreciation is also due to the Centre for High-Performance Computing (CHPC) in Cape Town for providing access to their remote computing resources, which enabled the successful completion of the computational work.

The input and output files generated from the CASTEP calculations that support the findings of this study are available from the corresponding author upon reasonable request.

References

1. C. W. Corti, The evolution of platinum jewellery alloys: from the 1920s to the 2020s: developments in new alloys and techniques. Johnson Matthey Technol. Rev. **66**, 418–434 (2022). https://doi.org/10.1595/205651322X16390711562364
2. T. Trosch, F. Lalire, S. Pommier, R. Völkl, U. Glatzel, Optimisation of a jewellery platinum alloy for precision casting: Evaluation of mechanical, microstructural and optical properties. Johnson Matthey Technol. Rev. **62**, 364–382 (2018). https://doi.org/10.1595/205651318X696837
3. D. Zito, V. Allodi, F. Trevisan, M. G. Rossini, A. Rossini, M. Mazza, Potential and Innovation of selective laser melting technique in platinum jewelry production. St. Fe

Symp. Jewel. Manuf. Technol. 625–684 (2018).
4. K. Lekganyane, M. Khodja-Moller, R. Mostert, D. Mkhonto, P. Maje, Structural, Thermodynamic and Elastic Properties of Binary FCC Pt-W and Pt-Ta Alloys—First-Principles Study, in Selected Articles from the 8th International Conference on Materials Engineering and Nanotechnology, ICMEN, Kuala Lumpur, Malaysia, September 28-29, September 28-29 (2024). https://doi.org/10.1007/978-981-96-3624-2_22
5. S. J. Clark, M.D. Segal, C.J. Pickard, P.J. Hasnip, M.I.J. Probert, K. Refson, M.C. Payne, First principles methods using CASTEP. Zeitschrift für Krist. Mater. **220**, 567–570 (2005). https://doi.org/10.1524/zkri.220.5.567.65075
6. M.D. Segall, P.J.D. Lindan, M.J. Probert, C.J. Pickard, P.J. Hasnip, S.J. Clark, M.C. Payne, First-principles simulation: ideas, illustrations and the CASTEP code. J. Phys. Condens. Matter. **14**, 2717 (2002). https://doi.org/10.1088/0953-8984/14/11/301
7. D. Vanderbilt, Soft self-consistent pseudopotentials in a generalized eigenvalue formalism. Phys. Rev. B **41**, 7892–7895 (1990). https://doi.org/10.1103/PhysRevB.41.7892
8. J. P. Perdew, Y. Wang, Accurate and simple analytic representation of the electron-gas correlation energy. Phys. Rev. B **45**, 13244 –13249 (1992). https://doi.org/10.1103/PhysRevB.45.13244
9. J. P. Perdew, K. Burke, M. Ernzerhof, Generalised gradient approximation made simple. Phys. Rev. Lett. **77**, 3865–3868 (1996). https://doi.org/10.1103/PhysRevLett.77.3865
10. T. H. Fischer, J. Almlof, General methods for geometry and wave function optimisation. J. Phys. Chem. **96**, 9768–9774 (1992). https://doi.org/10.1021/j100203a036
11. J. Yang, J. Huang, Z. Ye, D. Fan, S. Chen, Y. Zhao, First-principles calculations on structural energetics of Cu-Ti binary system intermetallic compounds in Ag-Cu-Ti and Cu-Ni-Ti active filler metals. Ceram. Int. **43**, 7751–7761 (2017). https://doi.org/10.1016/j.ceramint.2017.03.083
12. S. Chen, Y. Sun, Y.H. Duan, B. Huang, M.J. Peng, Phase stability, structural and elastic properties of C15-type laves transition-metal compounds MCo2 from first-principles calculations. J. Alloys Compd. **630**, 202–208 (2015). https://doi.org/10.1016/j.jallcom.2015.01.038
13. V. Stevanović, S. Lany, X. Zhang, A. Zunger, Correcting density functional theory for accurate predictions of compound enthalpies of formation: fitted elemental-phase reference energies. Phys. Rev. B **85**, 115104 (2012). https://doi.org/10.1103/PhysRevB.85.115104
14. M. Z. Rahaman, M. A. Rahman, Novel laves phase superconductor NbBe2: a theoretical investigation. Comput. Condens. Matt. **8**, 7–13 (2016). https://doi.org/10.1016/j.cocom.2016.06.001
15. J. F. Nye, *Propriétés physiques des cristaux*. Dunod, (1961)
16. G. Cizeron, Propriétés physiques des cristaux. Leur représentation par des tenseurs et des matrices, Bull. Minéralogie. **84**, 335 (1961). https://www.persee.fr/doc/bulmi_00379328_1961_num_84_3_5507_t1_0335_0000_5
17. M. Born, K. Huang, Dynamical Theory Of Crystal Lattices,(1996). https://doi.org/10.1093/oso/9780192670083.001.0001
18. R. Hill, The elastic behaviour of a crystalline aggregate. Proc. Phys. Soc. Sect. A **65**, 349 (1952). https://doi.org/10.1088/0370-1298/65/5/307

19. W. Voigt, Lehrbuch der kristallphysik (mit ausschluss der kristalloptik. BG Teubner, 1910).
20. A. Reuss, Z. Angew. Calculation of the flow limits of mixed crystals on the basis of the plasticity of monocrystals. Math. Mech. **9**, 49–58 (1929)
21. S. F. Pugh, XCII.Relations between the elastic moduli and the plastic properties of polycrystalline pure metals.Dublin Philos. Mag. J. Sci. **45**, 823–843 (1954). https://doi.org/10.1080/14786440808520496
22. Z. T. Y. Liu, D. Gall, S. V Khare, Electronic and bonding analysis of hardness in pyrite-type transition-metal pernitrides. Phys. Rev.. B **90**, 134102 (2014). https://doi.org/10.1103/PhysRevB.90.134102
23. N. N. Hoover, B. J. Auten, B. D. Chandler, Tuning supported catalyst reactivity with dendrimer-templated Pt−Cu nanoparticles. J. Phys. Chem. B **110** 8606–8612 (2006). https://doi.org/10.1021/jp060833x
24. Z. Sun, D. Music, R. Ahuja, J. M. Schneider, Theoretical investigation of the bonding and elastic properties of nanolayered ternary nitrides. Phys. Rev. B **71**, 193402 (2005). https://doi.org/10.1103/PhysRevB.71.193402
25. C. M. Zener, Elasticity and Anelasticity of Metal. J. Phys. Chem. **53**, 1468 (1949). https://doi.org/10.1021/j150474a017
26. S. I. Ranganathan, M. Ostoja-Starzewski, Universal Elastic Anisotropy Index Phys. Rev. Lett. **101**,055504 (2008). https://doi.org/10.1103/PhysRevLett.101.055504